Percolation and conductivity in evolving disordered media

Carl Fredrik Berg [*]

PoreLab, Department of Geoscience and Petroleum, Norwegian University of Science and Technology, Trondheim, Norway

Muhammad Sahimi

Mork Family Department of Chemical Engineering and Materials Science, University of Southern California, Los Angeles, California 90089-1211, USA

Percolation theory and the associated conductance networks have provided deep insights into the flow and transport properties of a vast number of heterogeneous materials and media. In practically all cases, however, the conductance of the networks' bonds remains constant throughout the entire process. There are, however, many important problems in which the conductance of the bonds evolves over time and does not remain constant. Examples include clogging, dissolution and precipitation, and catalytic processes in porous materials, as well as the deformation of a porous medium by applying an external pressure or stress to it that reduces the size of its pores. We introduce two percolation models to study the evolution of the conductivity of such networks. The two models are related to natural and industrial processes involving clogging, precipitation, and dissolution processes in porous media and materials. The effective conductivity of the models is shown to follow known power laws near the percolation threshold, despite radically different behavior both away from and even close to the percolation threshold. The behavior of the networks close to the percolation threshold is described by critical exponents, yielding bounds for traditional percolation exponents. We show that one of the two models belongs to the traditional universality class of percolation conductivity, while the second model yields nonuniversal scaling exponents.

I. INTRODUCTION

Percolation theory [1,2] has provided deep insights into the flow and transport properties of a vast number of heterogeneous materials and media and has found numerous applications [3] in a variety of contexts. In many cases the heterogeneous materials are represented by conductance networks [4], if a scalar transport process is to be studied; by a network of elastic elements, such as springs [5–7] or beams [8], if vector transport processes are investigated; or by a network of interconnected pores [9], if one is to examine various fluid flow phenomena in porous materials and media. When representing natural and industrial heterogeneous materials, the conductance of the bonds or pores might be distributed according to some probability distribution function that represents the morphology of the materials [10,11]. In practically all cases, however, the conductance of the network elements is modeled as constant throughout the percolation process under study.

There are, however, many important problems in which the conductance of the bonds in the networks that represent

the morphology of the system of interest evolves over time and, therefore, does not remain constant. One example is noncatalytic gas-solid reactions with solid products, such as sulphation of calcined limestone particles that are highly porous and contain a range of pore sizes,

$$CaO(s) + SO_2(g) + \tfrac{1}{2}O_2(g) \rightarrow CaSO_4(s).$$
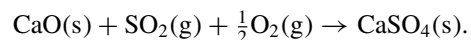
Numerous experiments indicate [12,13] that during the reaction the solid volume increases, and the pores are gradually plugged. Another example is the important problem of catalyst deactivation [14] in which a reactant reacts within the pore space of the catalyst and produces products that not only cover the catalyst's active sites but also precipitate on the solid surface of the pores and plug them, leading to deactivation of the catalyst. A third example is the transport of colloidal particles and stable emulsions in flow through a porous medium, during which the particles and emulsions precipitate on the surface of the pores and reduce their flow capacity [15–17]. The pore space of rock and other natural porous media evolve due to dissolution or precipitation. The fourth example is quartz cementation in sandstone that yields a pore space with a continuous range of various porosity and the corresponding flow and transport properties, such as permeability and electrical conductance. Another example is the evolution of sandstone pore structure in the near-well region by salt precipitation during CO_2 injection for its sequestration [18,19], as well as during evaporation of brine and the resulting salt precipitation [20–22]. Pore structure evolution is also observed in systems where the pore sizes of porous materials and, hence, their con-

ductances are reduced mechanically by, for example, applying an external stress or pressure to the material [23,24]. In all such cases, and numerous other examples, such as clogging of nanopores by transport of DNA [25], one has an evolving network.

Thus, the purpose of the present paper is to study the transport properties of evolving networks, particularly near their percolation threshold p_c. The goal of our study is twofold. One is to understand how the transport properties evolve in such networks, and how their evolution depends on the manner by which the conductances decrease. The second goal is to see whether the power law of percolation theory, according to which the effective conductivity σ_e follows the universal power law,

$$\sigma_e \propto (p - p_c)^t , \tag{1}$$

is also satisfied by the effective conductivity of evolving networks, where p is the fraction of the bonds with a nonzero conductance, and t is the critical exponent whose value is largely universal with $t \simeq 1.3$ in two dimensions.

The rest of this paper is organized as follows. In the next section, we introduce the models that we study and explain how they are employed in our numerical simulations. In Sec. III we present the details of the numerical simulations. Section IV presents the results for the power laws that the effective conductivity of the proposed models follow near the percolation threshold and compares them to the traditional models of random conductance networks. In Sec. V the implications of the results are discussed in detail, while the last section summarizes the results.

II. THE MODELS

The main motivation for this work is transport in evolving porous media, which typically occurs in complex three-dimensional pore networks. For the sake of more efficient simulations of very large networks, however, we restrict our study to the square lattice, which allows us to make precise comparisons with the existing models.

The simplest network we consider is the traditional square lattice in which we remove bonds by a probability p and where the remaining bonds have unit conductance. For straightforward comparison with models that will be introduced below, we define these networks in the following way [26]: We attribute a random number $p(e) \in [0, 1]$ to each bond $e \in E$, where E is the set of bonds in the initial graph, in our case the square lattice. This gives rise to a conductance map $g_o : E \to \mathbb{R}^+$ by letting

$$g_o(p, e) = \begin{cases} 1 & \text{if } p(e) \leqslant p \\ 0 & \text{if } p(e) > p \end{cases}. \tag{2}$$

Thus, we attribute unit conductance to all the bonds with a random number smaller than p, and zero conductance to the remaining bonds. A conductance map g defines a network, i.e., a weighted graph where the weights represent conductances. To simplify notation we let g represent both the conductance map and the network defined by this map. Networks g_o in which the bonds (or sites) are removed (make no contribution to transport) by a certain probability have been widely studied in the classical percolation theory and are well covered in the

literature [1–3]. They have many interesting properties with known behavior close to the percolation threshold p_c.

In the model above all bonds have unit conductance. Different transport processes have different relations to, e.g., the cross-sectional area available for transport. For example, the electrical conductance of a cylindrical pipe with a constant cross-sectional area and filled with an electrolyte is proportional to the cross-sectional area, whereas, according to the Hagen-Poiseuille equation, the fluid flow rate through the same cylindrical pipe due to a pressure difference is proportional to the cross-sectional area squared. If we view a bond as a cylindrical pipe of unit length and a variable volume V_b, then the cross-sectional area will be proportional to the volume, $A_b \propto V_b$. If a bond weight is assumed to represent its volume or mass, then different transport processes can be represented by raising the weight to a power. In this article we use mass instead of volume. For a porous medium, this can be thought of as the mass of the electrolyte or a fluid filling the volume, thereby equating the two through a constant electrolyte of fluid density.

Motivated by evolving porous media, we introduce two types of evolving networks. The first is similar to the networks defined by Eq. (2), but where we have a link weight that is inversely proportional to the probability that the bond is removed. The link weight is set to be equal to the mass and is expressed as

$$m_p(p, e) = \begin{cases} 1 - p(e) & \text{if } p(e) \leqslant p \\ 0 & \text{if } p(e) > p \end{cases}. \tag{3}$$

This type of network is related to clogging of a porous medium, such as a filter or membrane. The model also has a close correspondence with the aforementioned noncatalytic gas-solid reactions and catalyst deactivation when diffusion limits the rate of reaction. As a result, the sizes of the pores are not reduced uniformly. In all such processes, the phenomena begin in a fully connected network, but, over time, the size of the pores gradually decreases due to either a chemical reaction that produces solid products (as in diffusion-limited catalytic or noncatalytic reactions) or by the precipitation of particles on surface of the pores due to the physical interactions between the particles and the pore surface, as in the clogging problems.

The initial network before the onset of the closure process has a mass distribution where $1 - p(e)$ is the mass of bond e, and the blocking of a bond tends to happen at the least conductive bonds, i.e., the bonds with the smallest mass, thus the smallest $1 - p(e)$ values. As discussed above, when the link weight is considered as a mass (or volume), then the weight can be related to various types of transport processes through an exponent τ as $g_p^\tau(p, e) = m_p(p, e)^\tau$. As described above, $\tau = 1$ is related to electrical conductance, while $\tau = 2$ is related to fluid flow. For this type of network, the values of the bond conductance have constant value $[1 - p(e)]^\tau$ until removed depending on p. The conductance distribution for the network evolves, however, with p.

A third type of network is given by the following function:

$$m_s(p, e) = \begin{cases} p - p(e) & \text{if } p(e) \leqslant p \\ 0 & \text{if } p(e) > p \end{cases}, \tag{4}$$

which is a simple representation of a precipitation or dis-solution process, where the precipitation (or, equivalently, the dissolution) is similar throughout the network. This corresponds to the aforementioned catalytic or noncatalytic gas-solid in which diffusion plays no role, and only the ki-netics of the reactions are important. For a porous medium, the precipitation reduces the volume of the pores, thereby reducing the original mass $1 - p(e)$ by the same mass $1 - p$ throughout the network, resulting in a mass of $[1 - p(e)] - (1 - p) = p - p(e)$. Once again, we relate the mass to trans-port through the exponent τ as $g_s^\tau(p, e) = m_s(p, e)^\tau$. For this type of network, both the bond conductances and their distri-bution evolve with p.

For comparison to the evolving networks that we have introduced, we also consider more traditional networks with a uniform mass distribution between endpoints a and b, $U(a, b)$, with $0 \leqslant a < b \leqslant 1$. Each bond e has two associated proba-bilities, one for the probability $p(e) \in [0, 1]$ of being removed, and one for the mass $m(e) \in [a, b]$ being a random number between a and b. The model is then defined by

$$m_r(a, b) = \begin{cases} m(e) & \text{if } p(e) \leqslant p \\ 0 & \text{if } p(e) > p \end{cases}. \tag{5}$$

Here we keep only the end points from the distribution $U(a, b)$ in our notation. This mass model then gives rise to the conduc-tance model $g_r^\tau(a, b) = m_r(a, b)^\tau$, so that the mass distribution stays equal to $U(a, b)$ for all p, and, as a consequence, the conductance distribution does *not* evolve with p. Later in this paper, we will demonstrate that this type of network is similar to our evolving networks for a restricted range of p. As the properties of the $g_r^\tau(a, b)$ models are known in the literature [27–29], they will be valuable for comparison with our evolving networks.

Note that the unit conductance in the g_0 model means that we can equate the conductance map $g_0^\tau(p, e)$ to a mass model $m_0(p, e)$ for all τ. We drop the superscript τ for the g_0 models, as they are all equal.

III. COMPUTER SIMULATIONS

All calculations in this study were carried out using the Python programming language. The networks were stored as two lists, one for the vertices, or sites, and one for the edges, or bonds. The reason for using lists instead of, e.g., NumPy arrays (a Python library) is that they are used in several loops, where retrieving values from lists is faster than from arrays. The vertex list stores for each vertex the coordinates, the number of edges connected to the vertex, and the edges identification numbers. The edge list stores the edge identity, the associated random number $p(e) \in [0, 1]$, and the identification numbers for the two connected vertices.

Two opposite sides of the networks were considered as the inlet and outlet. For each network, we first determine the percolation threshold p_c, i.e., the smallest value of p such that the network $g_o(p)$ connects the inlet to the outlet. The threshold was computed by a binary search algorithm: The links are ordered according to their value of $p(e)$. We start the binary search by checking if $g_o(p)$ is connected when p equals the link value $p(e)$ in the middle of the stack. If

it is connected, we remove the upper half of the link stack; if not, we remove the lower half. We then check if $g_o(p)$ is connected for p equal to the link value $p(e)$ in the middle of the remaining stack. This process is continued until there is only one link left in the stack, yielding the bridging link at the percolating threshold. In addition, we check during the binary search whether the network is connected by first performing two breadth-first searches [30,31], one from the inlet and one from the outlet, and then checking the intersection of the resulting two searches; the network is connected if the intersection is nonzero.

To calculate the effective conductance of the networks, we follow the standard approach, namely, applying Kirchhoff's circuit laws. For each node i we have the equation

$$\sum_j g(e)(\phi_j - \phi_i) = 0, \tag{6}$$

where ϕ_i is the potential at node i, and e is the edge (i, j) for the set of nodes $\{j\}$ connected to i. The effective conductance is computed by representing the set of equations given by Eq. (6) in matrix form $\mathbf{M\Phi} = \mathbf{B}$ [4]. Here $\mathbf{B}$ is the vector representing the boundary conditions. As the boundary con-ditions, we applied a potential difference between the inlet and outlet. The matrix $\mathbf{M}$ represents the discretized Laplacian matrix for the network with the conductance values as weights for the bonds and is stored in compressed sparse column ma-trix format using the SciPy library. The matrix $\mathbf{M}$ was inverted using either the conjugate-gradient or the LU-decomposition method, both in the SciPy library, depending on the bandwidth of the matrix. We then obtained the solution vector $\mathbf{\Phi} = \mathbf{M}^{-1}\mathbf{B}$, which yields the potentials ϕ_i in the nodes, from which the total current through the network and, hence, the effective conductance is computed. Dividing the effective conductance by the network size we obtain the effective conductivity σ_e [1,3].

For well-connected networks, the approach was efficient and accurate. Close to the percolation threshold, however, where, due to the tortuous and constricted nature of the conducting paths, the current is very unevenly distributed in the network, the matrix inversion is susceptible to numer-ical errors. To reduce such numerical issues, we construct the Laplacian matrix $\mathbf{M}$ of the backbone, where we identify the backbone of the network by a method similar to Tar-jan's strongly connected components algorithm [30,31], but with a nonrecursive implementation in order to avoid stack overflow problems for large network sizes. For each network size, we generated at least 100 realizations and averaged the results.

IV. RESULTS AND DISCUSSION

We now investigate the evolving networks introduced in Sec. II, both theoretically and numerically. We carried out ex-tensive simulations in order to observe and study the behavior of the effective conductivity of the networks as they evolve.

A. Conductance functions g_o and g_p^τ

As is well known, near the percolation threshold p_c, the effective conductivity of the network g_o (i.e., the network
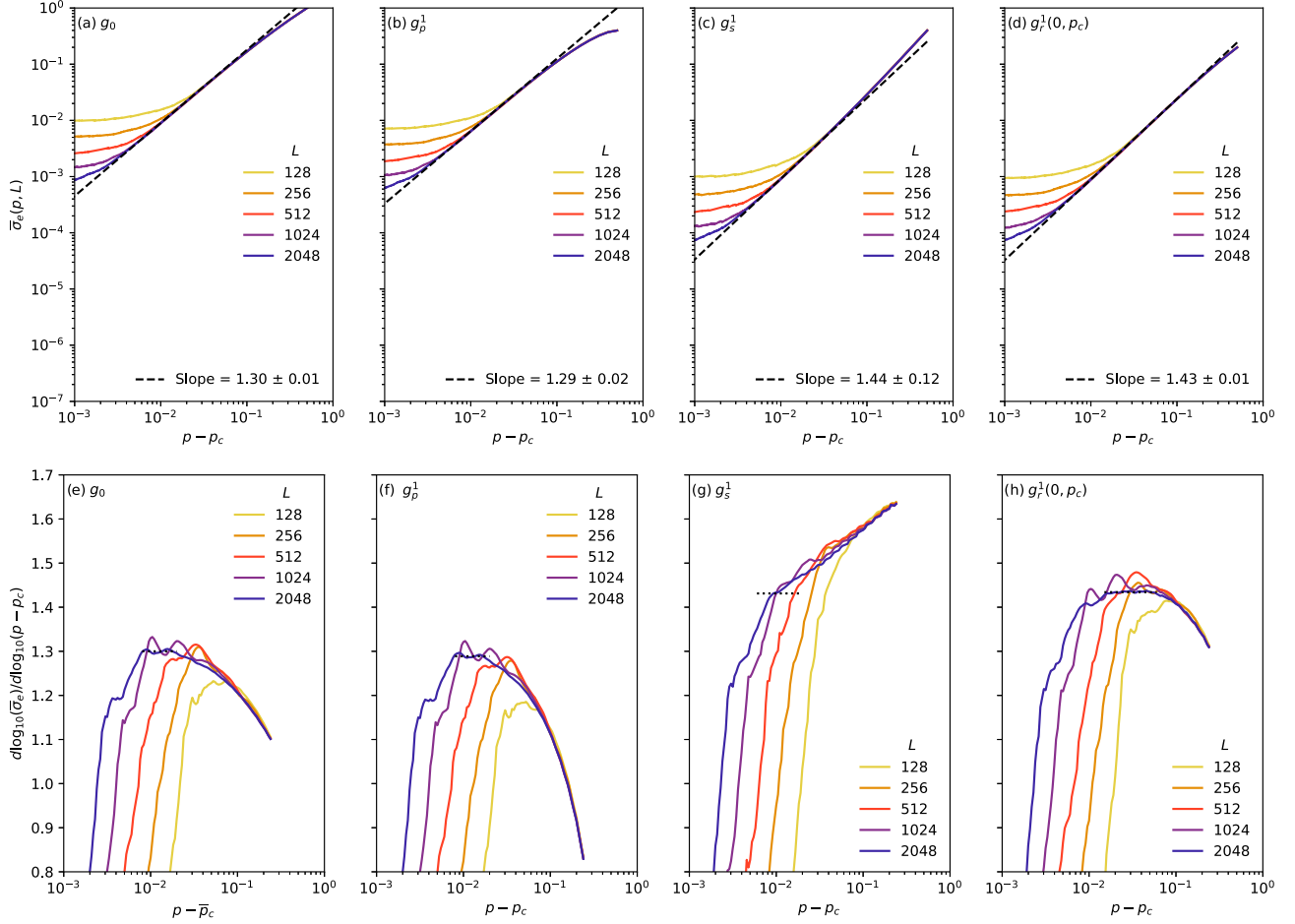
FIG. 1. Average effective conductivity σ_e for 100 realizations for each conductance map g^1 in (a)–(d), with the corresponding derivatives in (e) and (f). Note that for each of the 100 realizations we have used the same $p(e)$ distribution for the four different conductance maps. The slope is estimated in the range marked by the dotted line in the derivative plots, with the error estimates for the slopes being simply the difference between the minimal and maximal derivative value inside the given range. There is no plateau for the g_s^1 model, and the dashed line range for model g_s^1 in (g) was chosen to obtain a slope similar to the slope for model g_r^1.

resulting from the conductance map g_o) follows the power law given in Eq. (1) with a critical exponent $t \simeq 1.3$. Figure 1(a) presents the dependence of the average of the effective conductivity $\sigma_e^o(p, L)$ of 100 realizations of the networks of type $g_o(p)$, the standard percolation conductivity model, on both L, the linear size of the network, and $(p - p_c)$. Figure 1(e) shows the numerical derivatives of the curves in Fig. 1(a). We see that by increasing the size of the network the gradient reaches a plateau with a value close to 1.3 and, thus, g_o converge to a power law of type (1) with a slope $t \simeq 1.3$, in agreement with the theoretical expectation.

Next, we investigate the critical exponent for the conductance model g_p^τ by identifying an upper and lower bound for the exponent value. The individual bond conductances of g_o are always larger or equal to the bond conductances of g_p^τ for all $\tau \geqslant 0$, i.e., $g_o \geqslant g_p^\tau$ for $\tau \geqslant 0$. As a consequence of [32, Lemma 11.4], $g_o \geqslant g_p^\tau$ implies that $\sigma_e^o(p, L) \geqslant \sigma_e^p(p, L)$. If g_p^τ follows a universal power law of type (1) with exponent t_p, then $\sigma_e^p(p, L) \leqslant \sigma_e^o(p, L)$ implies that $t_p \geqslant t = 1.3$. Thus, we have identified a lower bound for the exponent t_p.

We now derive an upper bound for t_p. For all $p > 0$, the smallest bond conductance value in g_p^τ is $(1 - p)^\tau$. If we let pg_o denote the network with all bond conductances equal to p, then $g_p^\tau(p, L) > (1 - p)^\tau g_o(p, L)$ for all $p_c \leqslant p < 1$. For each τ, since $\sigma_e^p(1, L) > 0$, there exists an $\epsilon > 0$ such that $g_p^\tau(p, L) > \epsilon g_o(p, L)$ for all $p_c \leqslant p \leqslant 1$. The effective conductivity of ϵg_o is $\epsilon \sigma_e^o$, where σ_e^o is the effective conductivity of g_o. As the effective conductivity of ϵg_o and g_o are equal up to a scaling with ϵ, then ϵg_o has the same power-law exponent in Eq. (1) as g_o, namely, $t \simeq 1.3$. Using the same argument that was utilized for the lower bound, $\sigma_e^p(p, L) \geqslant \epsilon \sigma_e^o(p, L)$ implies that $t_p \leqslant t = 1.3$. Since we then have the same lower and upper bound for t_p, namely, $t \leqslant t_p \leqslant t$, we have $t_p = t \simeq 1.3$. Thus, networks of type g_p^τ follow the traditional critical behavior when $p \to p_c$.

Next, we consider an alternative method for estimating t_p. As $p \to p_c$, the mass distribution of g_p^τ will converge towards the distribution $p_c - p(e)$, where $p(e) \in U(p_c, 1)$. Thus, the mass distribution of g_p^τ converges towards the mass distribution of a network of type $g_r^\tau(p_c, 1)$, i.e., a g_r^τ function with $m(e) \in U(p_c, 1)$. The networks $g_r^\tau(p_c, 1)$ and g_p^τ are therefore
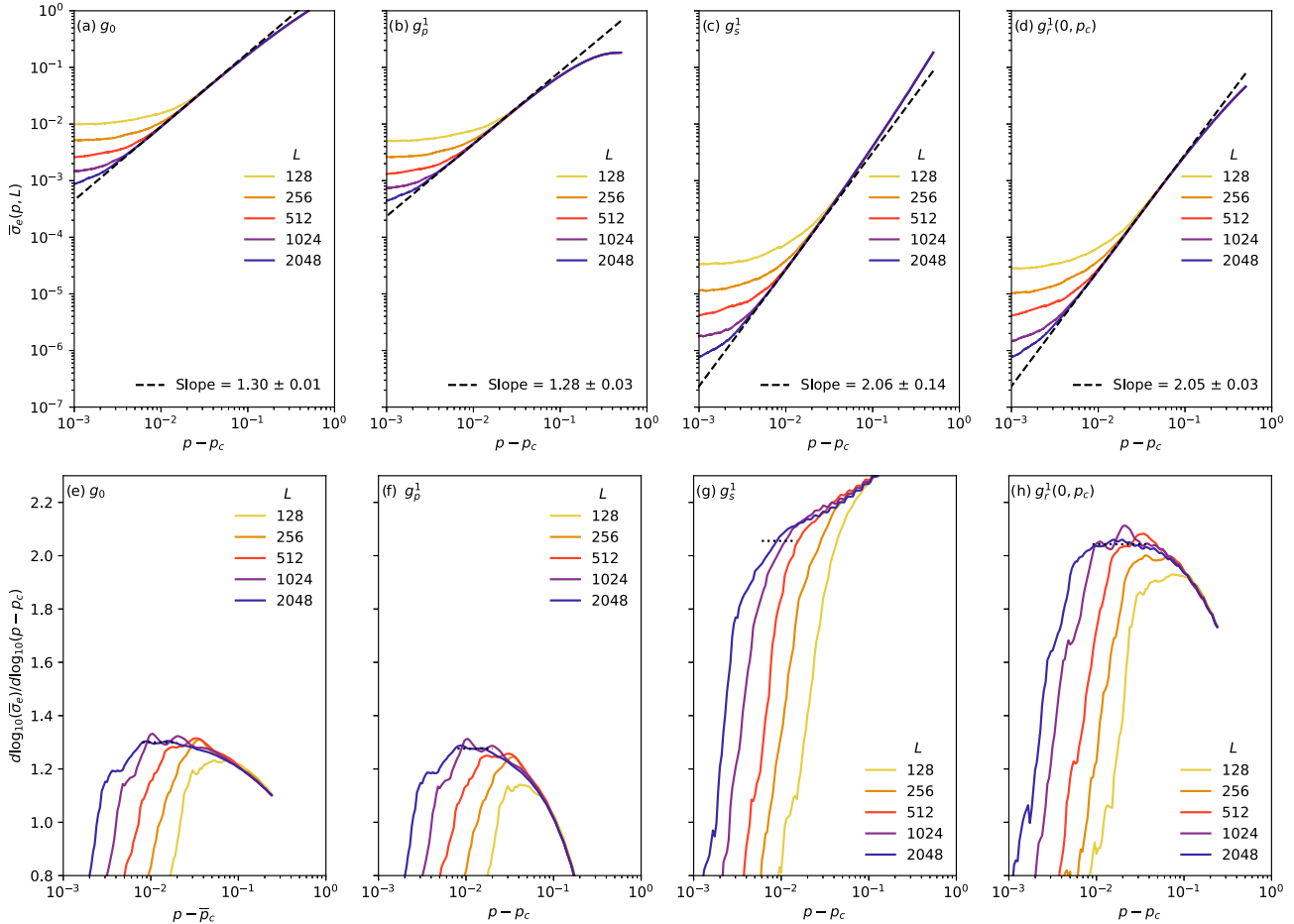
FIG. 2. Average effective conductivity σ_e for 100 realizations for each conductance map g^2 in (a)–(d), with the corresponding derivatives in (e) and (f). The slope is estimated in the range marked by the dotted line in the derivative plots, with the error estimates for the slopes being simply the difference between the minimal and maximal derivative value inside the given range. Note that the plots for g_o in (a) and (e) are equal to the corresponding ones in Fig. 1; however, their y scales differ. As with g_s^1, there is no plateau for the g_s^2 model, and the dashed line range for model g_s^2 was chosen to obtain a slope similar to the slope for model g_r^2.

expected to have the same properties when $p \to p_c$, including a similar critical exponent (this will be substantiated further in the discussion on g_s below). We have conducted simulations to confirm such a convergence.

We now use $g_r^\tau(p_c, 1)$ to obtain the power-law description for g_p^τ. The effective conductivity of $g_r^\tau(p_c, 1)$ is bounded from above by g_o and by $p_c^\tau g_o$ from below. Since $p_c^\tau g_o$ has the same critical exponent $t \simeq 1.3$ as g_o, then the critical exponent for $g_r^\tau(p_c, 1)$ is bounded from both above and below by $t \simeq 1.3$, and, thus, the exponent for $g_r^\tau(p_c, 1)$ is also $t \simeq 1.3$. As g_p^τ and $g_r^\tau(p_c, 1)$ converge when $p \to p_c$, they have the same critical exponents, which provides an alternative proof that $t_p \simeq 1.3$.

The results for t_p were verified by the simulations. Figures 1(b) and 1(f) present the average effective conductivity $\sigma_e^p(p, L)$ and its gradients for the model g_p^1. Similarly, we show the average effective conductivity and gradients for g_p^2 in Figs. 2(b) and 2(f). The inequality $\sigma_e^o(p, L) \geqslant \sigma_e^p(p, L)$ used to obtain the lower bound for t_p can be verified by comparing Fig. 1(a) with Fig. 1(b) and Fig. 2(b). The slope of the $\sigma_e^p(p, L)$ curves, both for $\tau = 1$ in Fig. 1(f) and for $\tau = 2$ in Fig. 2(f), converge towards a plateau. While the σ_e^o and σ_e^p

curves have different heights, the plateaus of their gradients have similar heights. It is seen that the plateau values for g_p^1 and g_p^2 are in good agreement with the theoretical value of 1.3. Note that the plots of the derivatives for the g_o and g_p^τ models have clear similarities, both for $\tau = 1$ and 2, as we use the same $p(e)$ distribution for the g_o and g_p^τ networks.

To further investigate the power laws for the various g functions, and in particular g_p, we consider finite-size scaling at p_c [1,3], namely, $\overline{g}_e(p_c) \propto L^{-t/\nu}$, where $\overline{g}_e(p_c)$ is the average effective conductivity $\sigma_e(p_c)$ at the percolation threshold p_c of a large number of network realizations, and ν is the critical exponent of percolation correlation length with $\nu = 4/3$ in two dimensions. We tested linear regression using both $L^{-\zeta}$ and curves with three free parameters of types suggested in [33]. The curve type yielding the best fit is of the form $L^{-\zeta}(a_1 - a_2/L)$ and is the plot type included in Fig. 3. Note that the other curve types, including $L^{-\zeta}$, yielded similar ζ exponents.

Figure 3 indicates that finite-size scaling yields an exponent of $\zeta = t/\nu \simeq 0.982$ for the standard percolation conductivity, corresponding to g_o, close to the expected value
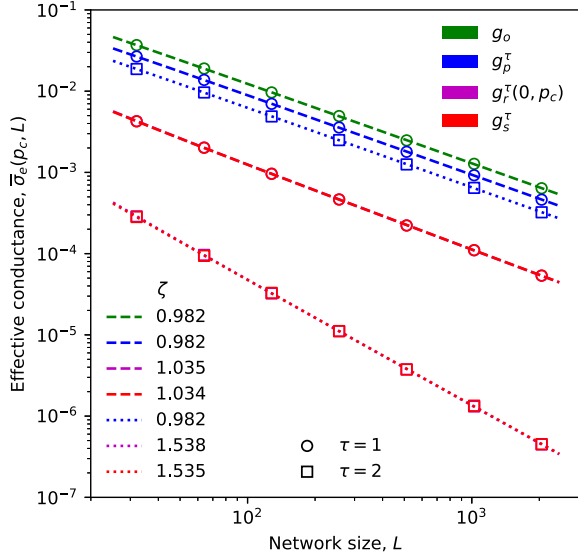
FIG. 3. Average effective conductivity σ_e at the theoretical percolation threshold $p_c = 0.5$ for more than 5000 realizations of each network size L. Note that the curve for g_r^τ is covered by the curve for g_s^τ, as they are basically indistinguishable.

of $t/\nu \simeq 0.975$. Note that $m_p^1 > m_p^2$ since $1 - p(e) < 1$ (see Eq. (3)) and, thus, $g_o > g_p^1 > g_p^2$, as observed in Fig. 3. As discussed above, we expect the same critical exponent for g_p^τ as for g_o. The models associated with g_p^τ yield slopes similar to that of g_o, and the computed $\zeta \approx 0.982$ are consistent with this expectation, yielding $t = \zeta\nu \simeq 1.31 \simeq 1.3$.

B. Conductance function g_s^τ

A critical difference between models g_s and g_p is that the conductance distribution of the bonds in g_s diverge, which can cause nonuniversal behavior [27,29]. Conductance distributions and nonuniversal behavior will be discussed in the next section. As in the alternative derivation of t_p, we will use functions of type g_r^τ to identify the critical exponents t_s for g_s^τ.

Let p_c^i be the individual percolation threshold for a given network [one realization of $p(e)$ values]. The link with $p(e) = p_c^i$ is the bridging link, e_b, which becomes a single

connection that keeps the network connected when approaching the individual percolation threshold p_c^i. When e_b is removed at $p = p_c^i$, the remaining network will be disconnected. The conductance of the bridging link will be $(p - p_c^i)^\tau \to 0$ when $p \to p_c^i$, whereas for all other links the conductance $[p - p(e)]^\tau$ converges to a positive constant. Since the remainder of the network has finite conductance when $p \to p_c^i$, the resistance of the bridging link will dominate the resistance of the full network in the limit $p \to p_c^i$. Thus, the effective conductivity scales as $\sigma_e \propto (p - p_c^i)^\tau L^{2-d}$, when $p \to p_c^i$ for networks of spatial dimension d. In Fig. 4(a) we present the effective conductivity of both g_s^1 and $g_r^1(0, p_c)$, indicating that the conductivity of g_s^τ converges to the slope given by τ, as expected from the derivation above.

If we consider a two-dimensional network g' in which all other links than e_b in g_s are replaced by superconductors, then the network g' will have a conductivity $\sigma_e' \propto (p - p_c^i)^\tau$ when $p \to p_c^i$. Thus, the development of the conductivity is of the power-law type Eq. (1) with critical exponent τ. Since the effective conductivity of g' is larger than the conductivity of g_s^τ, i.e., $\sigma_e' > \sigma_e^s$, we see that the critical exponent t_s must be bounded below as $t_s \geqslant \tau$. Note that, as the conductivity of g_s^τ is always smaller than the conductivity of g_o when $\tau > 0$, $\sigma_e^o > \sigma_e^s$, we also have $t_s \geqslant t = 1.3$. Thus, in general, we have, $t_s \geqslant \max(t, \tau)$, giving a lower bound for t_s.

Consider the situation in which $L \gg \xi$, i.e., one in which L is large compared to the correlation length ξ of percolation. In this limit there are no singly-connected bonds; according to [1] the minimum cut contains approximately L/ξ bonds. As the network is well connected when $L \gg \xi$, we can disregard the effect of the conductance of e_b vanishing when $p \to p_c^i$, as e_b is then on one of many connected paths in the infinite percolation cluster. The network will have a mass distribution equivalent to that in $g_r^\tau(0, p_c^i)$ when $p \to p_c^i$. To compare our network to $g_r^\tau(0, p_c)$, we need $p \simeq p_c$ for the distribution of bond conductances in g_s^τ to be similar to that in $g_r^\tau(0, p_c)$. This requirement does not, however, scale with L, so that we can expect the two conductance distributions g_s^τ and $g_r^\tau(0, p_c)$ to converge at the same values of p, independent of the size L. Therefore, for large L we can expect a region of p values where $g_s^\tau \simeq g_r^\tau(0, p_c)$, i.e., where $L \gg \xi$ and $p \simeq p_c$.
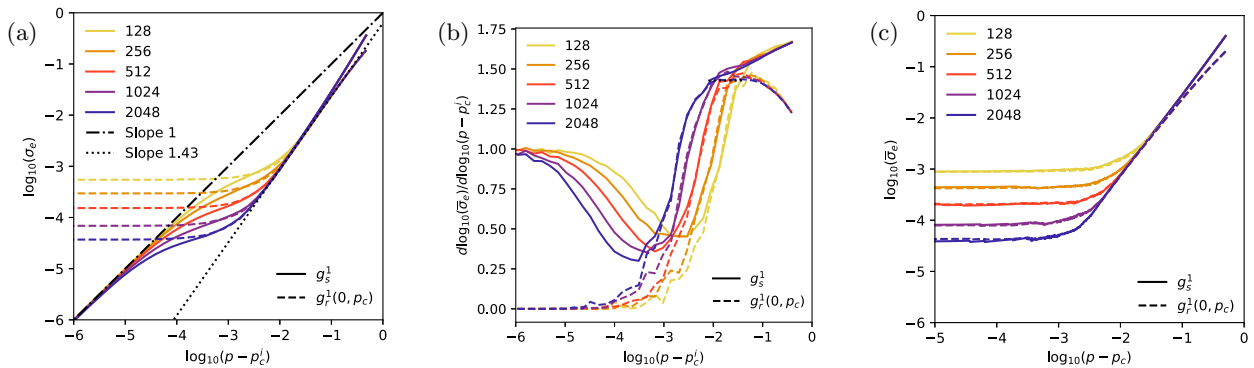

FIG. 4. (a) Average effective conductivity σ_e for the same 100 realizations as used in Fig. 1(c) and 1(d). They are, however, plotted for the convergence towards their individual thresholds $p - p_c^i$. (b) Numerical derivatives of the curves in (a), with the dashed line indicating the plateau of the $g_r^1(p_c, 1)$ curves. The plot in (c) is using the global percolation threshold p_c, instead of the individual percolation thresholds p_c^i.

In Fig. 4 we present the results for both g_s^1 and $g_r^1(0, p_c)$. As seen in the figure, g_s^1 and $g_r^1(0, p_c)$ differ for both large and small values of $p - p_c^i$; they are, however, similar for a range of intermediate values that correspond to the region in which $L \gg \xi$ and $p \simeq p_c$. We also observe that the two curves diverge when $p \to p_c^i$: In this case, we have $L \ll \xi$ and, thus, the link e_b will become the single bridging link. Since the weight $g_s^\tau(p, e_b) \to 0$ when $p \to p_c^i$, this conductance will begin dominating the overall conductance of the network as described above, and the conductance will vanish by the power law, $\sigma_e^s \propto (p - p_c^i)^\tau$, as $p \to p_c^i$. This is in contrast to the g_r^τ network, for which the bridging link e_b has a finite conductance, $g_r^\tau(p, e_b) > 0$ and, thus, σ_e^r converges to a finite value when $p \to p_c^i$. The two conductance descriptions g_s^τ and g_r^τ must, therefore, begin to diverge when $p \to p_c^i$, and Fig. 4 indicates that they do.

While the conductivities have clearly different trajectories when plotted versus their individual percolation thresholds p_c^i, the difference becomes insignificant when one uses instead the traditional averaging $p - p_c$, where p_c is the percolation threshold for an infinite network. Let $p_{av} = \langle p_c^i \rangle$ be the average of the percolation thresholds for the individual networks, and let $\Delta = \sqrt{\langle (p_c^i)^2 \rangle - \langle p_c^i \rangle^2}$ be the standard deviation of the individual percolation thresholds. The two values are known to scale as $p_{av} - p_c \propto L^{-1/\nu}$ and $\Delta \propto L^{-1/\nu}$ [1, p. 73]. The standard deviation of the individual percolation thresholds Δ is larger than the difference between p_{av} and p_c; thus, the $\Delta \propto L^{-1/\nu}$ correspondence will be of importance to us. The difference between the g_s^τ and $g_r^\tau(0, p_c)$ models when $p \to p_c^i$ is expected to be reflected in the $p - p_c$ curves only if Δ is smaller than the onset of divergence between the g_s and g_r curves. In Fig. 4(c) we have plotted the results for $p - p_c$. There is no evident difference between the curves, indicating that Δ is larger than the onset of the divergence observed in Fig. 4(a) and 4(b).

Based on the above derivations, the power laws for g_s and g_r are expected to be the same, and should be bounded from below by $\max(t, \tau)$. This is corroborated by the results in Fig. 3, where the results for $g_r^\tau(0, p_c)$ and g_s^τ are almost identical for both values of τ. For $\tau = 1$ they indicate $\zeta = t_s/\nu \simeq 1.034$, which yields a nonuniversal scaling exponent of $t_s \simeq 1.38 \geqslant t = \max(t, \tau)$. For $\tau = 2$ we have $\zeta \simeq 1.535$, yielding $t_s \simeq 2.05 \geqslant \tau = \max(t, \tau)$.

The results for g_s^1 are presented in Figs. 1(c) and 1(g), and those for g_s^2 are shown in Figs. 2(c) and 2(g). Since $g_o > g_p^\tau > g_r^\tau$, we have $\sigma_e^o > \sigma_e^p > \sigma_e^r(0, p_c)$. It is evident from Fig. 1(g) that even the largest network size, $L = 2048$, does not produce a plateau for the gradient. We thus plot $g_r^1(0, p_c)$ in Figs. 1(d) and 1(h). The derivative indicates a plateau, however, at a value around $t_s \simeq 1.43$. This is higher than, $t_s = 1.38$, obtained from the finite-size scaling above. For $\tau = 2$, as seen in Figs. 1(d) and 1(h), we obtain a slope of $t_s \simeq 2.05$, which is in agreement with the finite-size scaling above. These results will be discussed further in the next section.

V. DISCUSSION

In the previous section, we investigated the power laws for the effective conductivity of evolving networks, g_p^τ and g_s^τ, introduced in this paper. We argued that the effective
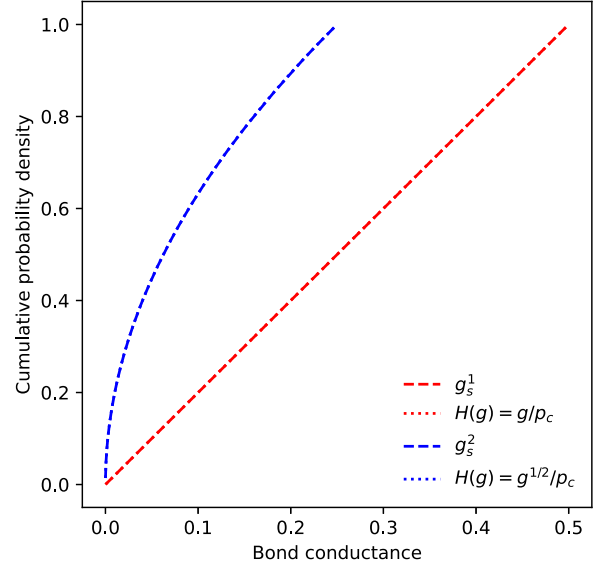

FIG. 5. Cumulative conductance distribution for g_s^τ for 100 realizations of size $L = 512$, together with the functional relationships describing the distribution for $g_r^\tau(0, p_c)$. The functional relationships are covered by distributions for g_s^τ

conductivities of these networks follow the same power laws as the networks $g_r^\tau(p_c, 1)$ and $g_r^\tau(0, p_c)$, respectively.

Nonuniversality has been observed for networks whose distribution of bond conductances diverges when the conductance values go to zero [27,29]. For $g_r^\tau(0, p_c)$ we have a uniform distribution of bond mass values in the range $[0, p_c]$, and the conductance for a bond of mass m is $g = m^\tau$. The probability of having a mass smaller than m is m/p_c. Thus, the probability of having a conductance smaller than $g = m^\tau$ becomes $m/p_c = g^{1/\tau}/p_c$, and the cumulative conductance distribution is given by

$$H(g) = g^{1/\tau}/p_c, \tag{7}$$

for $g \in (0, p_c^\tau)$. In Fig. 5 we present the conductance distribution in g_s^τ for the backbone at $p = p_c$, together with the distribution function in Eq. (7). We observe an equivalent distribution for g_s^τ as $g_r^\tau(0, p_c)$.

If we scale the conductances in the range $(0, p_c^\tau = 2^{-\tau})$ to the range $(0,1)$ [with the above notation, we, thus, consider $p_c^{-\tau} g_r^\tau(0, p_c)$], we have the cumulative probability $H(g) = g^{1/\tau}$, which yields the probability distribution

$$h(g) = \frac{1}{\tau} g^{1/\tau - 1} = (1 - \alpha) g^{-\alpha}, \tag{8}$$

where the last term is on the form used in [27], obtained from $\alpha = 1 - 1/\tau$. For $\tau > 1$ we have a negative exponent for g in Eq. (8), making $h(g)$ diverge when the conductance $g \to 0$. According to [27], we then have $\sigma_e \propto (p - p_c)^{t_r}$, where $t_r = t + \alpha/(1 - \alpha) = t + \tau - 1$, with t being the standard conductivity exponent, with $t \simeq 1.3$ for two-dimensional networks, as mentioned above. Note also that other authors reported different values for t_r, with $0 < t_r - t < 3/2$ for $\tau = 2$ according to [29]. In [28] the nonuniversal exponent is given as $t_r = \max(t, (1 - \alpha)^{-1}) = \max(t, \tau)$, which is exactly the lower bound we obtained for g_s above.

For $\tau = 1$ the literature indicates that for the g_r^τ model $t_r = t \simeq 1.3$. Our derivations above should have yielded $t_s = t_r = t$, but our numerically computed values for t_s are higher than this, with $t_s \simeq 1.38$ by finite-size scaling and $t_s \simeq 1.43$ through investigating the gradient of the curves $g_s(L, p)$. It has been reported that the universality constant for t_r is difficult to obtain as logarithmic corrections set in for $\tau = 1$ [28]. Our computed values are, however, in excellent agreement with estimates from similar numerical simulations for the g_r^τ model [34].

For $\tau = 2$, the literature differs on the value of t_r, with $1.3 < t_r < 2.8$ according to [29], $t_r \simeq 2.3$ according to [27], and $t_r = 2$ according to [28]. Our estimate of $t_s \simeq 2.05$ is within the spread of the t_r values for the g_r^τ model, as indicated by the aforementioned authors.

VI. SUMMARY

We introduced two types of evolving networks that are related to natural and industrial processes, such as clogging, precipitation, and dissolution. One model, g_p^τ, represents clogging processes that tend to block the lowest conducting bonds. The second model, g_s^τ, represents precipitation processes that reduce the conductance of all bonds similarly. The mass distribution is linked to the conductance by the exponent τ, where $\tau = 1$ represents electrical conductance or diffusion, while $\tau = 2$ represents fluid flow.

The effective conductivity of the models that we introduced behaves differently from that of the traditional networks g_o with constant bond conductance. We showed, however, that the power laws $\sigma_e^p \propto (p - p_c)^{t_p}$ for g_p^τ still belong to the standard universality class with exponent $t_p = t \simeq 1.3$.

The effective conductivity of the g_s^τ model follows a power law similar to $g_r^\tau(0, p_c)$. The effective conductivity of the $g_r^\tau(0, p_c)$ model is known in the literature to have nonuniversal power laws near the percolation threshold, and we have the same nonuniversality for g_s^τ. The conductivity of the g_s^τ model has, however, a radically different behavior than $g_r^\tau(0, p_c)$, when we consider convergence towards individual percolation thresholds, $p \rightarrow p_c^i$. In this limit the g_s^τ conductivity scales as $\sigma_e^s \propto (p - p_c^i)^\tau$, which leads to a lower bound $t_s \geqslant \max(t, \tau)$ for the power law, $\sigma_e^s \propto (p - p_c)^{t_s}$. As the effective conductivity of both g_s and $g_r(0, p_c)$ follow the same power laws, this yields the same lower bound for $g_r^\tau(0, p_c)$, namely, the lower bound $t_r \geqslant \max(t, \tau)$.

[1] D. Stauffer and A. Aharony, *Introduction to Percolation Theory* (Taylor & Francis, London, 2003).

[2] A. A. Saberi, Recent advances in percolation theory and its applications, Phys. Rep. **578**, 1 (2015).

[3] M. Sahimi, *Applications of Percolation Theory*, 2nd ed. (Springer, New York, 2023).

[4] S. Kirkpatrick, Percolation and conduction, Rev. Mod. Phys. **45**, 574 (1973).

[5] S. Feng and P. N. Sen, Percolation on Elastic Networks: New Exponent and Threshold, Phys. Rev. Lett. **52**, 216 (1984).

[6] S. Feng, P. N. Sen, B. I. Halperin, and C. J. Lobb, Percolation on two-dimensional elastic networks with rotationally invariant bond-bending forces, Phys. Rev. B **30**, 5386 (1984).

[7] S. Feng and M. Sahimi, Position-space renormalization for elastic percolation networks with bond-bending forces, Phys. Rev. B **31**, 1671 (1985).

[8] T. Lewinski, Dynamical tests of accuracy of Cosserat models for honeycomb gridworks, Z. Angew. Math, Mech. **68**, T197 (1988).

[9] M. Sahimi, *Flow and Transport in Porous Media and Fractured Rock: From Classical Methods to Modern Approaches* (John Wiley & Sons, 2011).

[10] I. Balberg, Recent developments in continuum percolation, Philos. Mag. B **56**, 991 (1987).

[11] I. Balberg, Continuum percolation, in *Encyclopedia of Complexity and Systems Science*, edited by R. A. Meyers (Springer, New York, 2009), pp. 1443–1475.

[12] S. Reyes and K. F. Jensen, Percolation concepts in modelling of gas-solid reactions—III. Application to sulphation of calcined limestone, Chem. Eng. Sci. **42**, 565 (1987).

[13] N. Shah and J. M. Ottino, Transport and reaction in evolving, disordered composites—II. Coke deposition in a catalytic pellet, Chem. Eng. Sci. **42**, 73 (1987).

[14] M. Sahimi and T. T. Tsotsis, A percolation model of catalyst deactivation by site coverage and pore blockage, J. Catal. **96**, 552 (1985).

[15] S. D. Rege and H. S. Fogler, Network model for straining dominated particle entrapment in porous media, Chem. Eng. Sci. **42**, 1553 (1987).

[16] M. Sahimi and A. O. Imdakm, Hydrodynamics of Particulate Motion in Porous Media, Phys. Rev. Lett. **66**, 1169 (1991).

[17] L. M. Schwartz, D. J. Wilkinson, M. Bolsterli, and P. Hammond, Particle filtration in consolidated granular systems, Phys. Rev. B **47**, 4953 (1993).

[18] R. Miri and H. Hellevang, Salt precipitation during CO$_2$ storage—A review, Int. J. Greenhouse Gas Control **51**, 136 (2016).

[19] J. Jeddizahed and B. Rostami, Experimental investigation of injectivity alteration due to salt precipitation during CO$_2$ sequestration in saline aquifers, Adv. Water Resour. **96**, 23 (2016).

[20] M. Norouzi Rad, N. Shokri, and M. Sahimi, Pore-scale dynamics of salt precipitation in drying porous media, Phys. Rev. E **88**, 032404 (2013).

[21] M. N. Rad, N. Shokri, A. Keshmiri, and P. J. Withers, Effects of grain and pore size on salt precipitation during evaporation from porous media, Transp. Porous Media **110**, 281 (2015).

[22] H. Dashtian, N. Shokri, and M. Sahimi, Pore-network model of evaporation-induced salt precipitation in porous media: The effect of correlations and heterogeneity, Adv. Water Resour. **112**, 59 (2018).

[23] S. Richesson and M. Sahimi, Flow and transport properties of deforming porous media. II. Electrical conductivity, Transp. Porous Media **138**, 611 (2021).

[24] S. Richesson and M. Sahimi, Flow and transport properties of deforming porous media. I. Permeability, Transp. Porous Media **138**, 577 (2021).

[25] T. Kubota, K. Lloyd, N. Sakashita, S. Minato, K. Ishida, and T. Mitsui, Clog and release, and reverse motions of DNA in a nanopore, Polymers **11**, 84 (2019).

[26] G. Grimmett, *Percolation* (Springer, 1999).

[27] P. M. Kogut and J. P. Straley, Distribution-induced non-universality of the percolation conductivity exponents, J. Phys. C **12**, 2151 (1979).

[28] J. P. Straley, Non-universal threshold behaviour of random resistor networks with anomalous distributions of conductances, J. Phys. C **15**, 2343 (1982).

[29] S. Feng, B. I. Halperin, and P. N. Sen, Transport properties of continuum systems near the percolation threshold, Phys. Rev. B **35**, 197 (1987).

[30] R. Tarjan, Depth-first search and linear graph algorithms, SIAM J. Comput. **1**, 146 (1972).

[31] A. P. Sheppard, M. A. Knackstedt, W. V. Pinczewski, and M. Sahimi, Invasion percolation: New algorithms and universality classes, J. Phys. A: Math. Gen. **32**, L521 (1999).

[32] H. Kesten, *Percolation Theory for Mathematicians*, Progress in Probability and Statistics Vol. 2 (Springer, New York, 1982).

[33] M. Sahimi and S. Arbabi, On correction to scaling for two-and three-dimensional scalar and vector percolation, J. Stat. Phys. **62**, 453 (1991).

[34] F. Flukiger, F. Plouraboué, and M. Prat, Nonuniversal conductivity exponents in continuum percolating Gaussian fractures, Phys. Rev. E **77**, 047101 (2008).